Transmembrane domain–dependent partitioning of membrane proteins within the endoplasmic reticulum

Paolo Ronchi,[1,2] Sara Colombo,[1,2] Maura Francolini,[1,2] and Nica Borgese[1,2,3]

[1]Consiglio Nazionale delle Ricerche, Institute of Neuroscience, Cellular and Molecular Pharmacology, University of Milan, 20129 Milan, Italy
[2]Department of Medical Pharmacology, University of Milan, 20129 Milan, Italy
[3]Faculty of Pharmacy, University of Catanzaro Magna Graecia, 88021 Roccelletta di Borgia (CZ), Italy

The length and hydrophobicity of the transmembrane domain (TMD) play an important role in the sorting of membrane proteins within the secretory pathway; however, the relative contributions of protein–protein and protein–lipid interactions to this phenomenon are currently not understood. To investigate the mechanism of TMD-dependent sorting, we used the following two C tail–anchored fluorescent proteins (FPs), which differ only in TMD length: FP-17, which is anchored to the endoplasmic reticulum (ER) membrane by 17 uncharged residues, and FP-22, which is driven to the plasma membrane by its 22-residue-long TMD. Before export of FP-22, the two constructs, although freely diffusible, were seen to distribute differently between ER tubules and sheets. Analyses in temperature-blocked cells revealed that FP-17 is excluded from ER exit sites, whereas FP-22 is recruited to them, although it remains freely exchangeable with the surrounding reticulum. Thus, physicochemical features of the TMD influence sorting of membrane proteins both within the ER and at the ER–Golgi boundary by simple receptor-independent mechanisms based on partitioning.

Introduction

The defined molecular composition of each compartment of the exo–endocytic pathway is generated by complex sorting mechanisms that determine which molecules are specifically recruited into, or excluded from, the anterograde or retrograde transport carriers that operate in intercompartmental traffic. For example, at the interface between the ER and the Golgi complex, exported cargo is packaged into coat protein complex (COP) II–coated carriers, whereas ER residents that have escaped by bulk flow are retrieved by COPI-coated retrograde vesicles. In addition, many resident proteins appear to avoid bulk flow by so-called static retention mechanisms that exclude them from COPII-coated carriers and, similarly, exported proteins are presumably kept out of retrograde vesicles that would otherwise return them to the ER (for review see Bonifacino and Glick, 2004).

Although packaging into transport carriers is generally signal-mediated and involves direct or indirect interactions between the cargo protein and coat components (for reviews see Bonifacino and Glick, 2004; Lee et al., 2004), a mechanism based on recognition between sorting signals and receptors is less likely to underlie exclusion events. Indeed, receptors involved in packaging, because of the different environments they encounter during transport, can first bind and then release their cargo and, thus, be reutilized many times. Instead, hypothetical retention receptors would remain permanently exposed to the environment of the donor compartment and would thus have to be present in stoichiometric ratios to their ligands. More importantly, they themselves would have to be kept out of transport vesicles, shifting the problem of the exclusion mechanism from the retained substrate to its receptor. For this reason, self-organizational principles, based on physicochemical features of retained proteins, must in the end be invoked to explain sorting by exclusion mechanisms. One such feature, involved in sorting of membrane proteins, is the length/hydrophobicity of the transmembrane domain (TMD).

TMD-dependent sorting has been observed essentially throughout the entire exo–endocytic pathway between the Golgi complex, the plasma membrane and post-Golgi intracellular compartments, and at the ER–Golgi interface (Bulbarelli et al., 2002; Nufer et al., 2003; Sato et al., 2003; Schamel et al., 2003). Although specific residues or sequence motifs are involved in some cases (Fiedler and Rothman, 1997; Dunbar et al., 2000;

Correspondence to Nica Borgese: n.borgese@in.cnr.it

Abbreviations used in this paper: COP, coat protein complex; cyt, cytochrome; D, diffusion coefficient; ERES, ER exit site; ERGIC, endoplasmic reticulum–Golgi intermediate compartment; FI, fluorescence intensity; FP, fluorescent protein; IC, intermediate compartment; M_f, mobile fraction; Rtn, reticulon; TA, tail anchored; TMD, transmembrane domain; VSVG, ts045 vesicular stomatitis virus glycoprotein.

The online version of this paper contains supplemental material.

The Journal of Cell Biology, Vol. 181, No. 1, April 7, 2008 105–118
http://www.jcb.org/cgi/doi/10.1083/jcb.200710093

Wang et al., 2002), this type of sorting is more commonly sequence-independent, with an observed correlation between increased TMD length/hydrophobicity and sorting to later stations of the secretory pathway (Bretscher and Munro, 1993; Bulbarelli et al., 2002; Karsten et al., 2004). Because the membranes of the secretory pathway become thicker and more rigid from the ER toward the cell surface (for review see Sprong et al., 2001), this correlation might reflect a thermodynamic advantage for protein-lipid assemblies in which TMDs and bilayers are hydrophobically matched (Bretscher and Munro, 1993; Dumas et al., 1999).

TMD-dependent sorting could, in principle, be based on recruitment into and/or exclusion from transport carriers of the substrate protein. At the ER–Golgi interface, the first of these mechanisms operates via a retrieval receptor, rer1p, which, by recognizing general features of the TMD, recruits escaped ER residents into retrograde vesicles (Fullekrug et al., 1997; Sato et al., 1997, 2003; Letourneur and Cosson, 1998). An involvement of the second mechanism, exclusion from anterograde vesicles, has also been suggested (Pedrazzini et al., 2000; Pentcheva et al., 2002; Schamel et al., 2003) but firm evidence in support of this is lacking. Analogous to what was hypothesized for Golgi proteins (Bretscher and Munro, 1993), such exclusion could be based on simple partitioning of the TMD into lipid domains that differ from the bilayer of budding transport carriers.

During the past years, our group has used C tail–anchored (TA) proteins as models to investigate the molecular basis of TMD-dependent sorting at the ER–Golgi interface. Because of their simple topology, consisting of a cytosolic N-terminal region, followed by a TMD very close to the C terminus (for review see Borgese et al., 2003), these proteins have clearly revealed a role for the TMD in keeping resident membrane proteins from escaping to downstream compartments. When the short and moderately hydrophobic TMDs of resident TA proteins are mutated to longer and more hydrophobic ones, the resulting protein variants escape from the ER and reach the plasma membrane. This effect is sequence independent (Honsho et al., 1998; Bulbarelli et al., 2002) and is transferable to fusion proteins, in which the cytosolic domain of the native protein is substituted with GFP (for review see Borgese et al., 2003). An open question is whether the sorting occurs by retrieval from retrograde transport carriers or by exclusion from anterograde transport carriers.

We previously demonstrated that cytochrome (cyt) b5, a TA protein that resides in the ER by a TMD-dependent mechanism, recycles very slowly through the cis-Golgi, suggesting that it is held back by mechanisms operating early at the ER–Golgi interface (Pedrazzini et al., 2000). To investigate these mechanisms, we have now compared the very early steps of trafficking of two model TA proteins that, because of their different TMD length, have different destinations within the secretory pathway (Bulbarelli et al., 2002). We find that the two proteins are partially segregated from each other already within the ER, showing different distributions between ER tubules, sheets, and exit sites. Because both constructs are freely diffusible, these results cannot be explained by their inclusion in large supramolecular protein assemblies but are instead consistent with simple partitioning effects based on different physicochemical differences between ER subdomains.

Results

Microinjected fluorescent protein (FP)–22 is visualized in the ER at early time points after microinjection of the cDNA and exits the ER by a COPII-dependent mechanism

In previous work, we showed that GFP-TA constructs, like the ones illustrated in Fig. 1 a, are sorted differently within the secretory pathway. A construct bearing the TMD of cyt b5 (FP-17) resides in the ER, whereas one with a lengthened TMD (FP-22) escapes from the ER and localizes to the plasma membrane and Golgi region of transfected cells (Bulbarelli et al., 2002). To visualize FP-22 while still in the ER and, thus, image the early steps of TMD-dependent sorting, we generated a pulse of synchronized expression of the two constructs by microinjecting cell nuclei with the corresponding cDNAs. As shown in Fig. 1 b (left), imaging of cells at short times (1 h) after the microinjection permitted visualization of both constructs in the ER. After a further 30 min in the presence of cycloheximide, FP-22 was seen to concentrate in the Golgi region (middle), and 1 h later it had decreased in the Golgi and moved to the plasma membrane (right). In contrast, FP-17 in the same cells remained in the ER at all time points.

Because some proteins may exit the ER by COPII-independent pathways (Hasdemir et al., 2005; Jüschke et al., 2005; Karhinen et al., 2005), we investigated whether FP-22 export is inhibited by a dominant-negative (H79G) form of Sar1 that blocks budding of COPII-coated vesicle at ER exit sites (ERES; Aridor et al., 1995). To this end, we microinjected the FP-22 coding plasmid into cells that had been transfected 12 h earlier with H79G-Sar1 cDNA. To identify the transfected cells, soluble YFP cDNA was transfected together with the Sar1 construct. As shown in Fig. 1 c, in transfected cells (left and middle), FP-22 failed to be exported and was totally localized in the ER even at 6 h after microinjection, whereas in the untransfected cells (right) it was efficiently transported to the plasma membrane. A similar COPII dependency for FP-22 export was shown under conditions of acute dominant-negative Sar1 inhibition in cells doubly microinjected with H79G-Sar1 protein in the cytoplasm and FP-22 cDNA in the nucleus (unpublished data).

Temperature blocks demonstrate sorting of FP-17 and -22 at ERES

To investigate whether the ER residency of FP-17 is caused by recycling from the intermediate compartment (IC), we incubated microinjected cells at 15°C, a temperature that causes accumulation of both exported and recycling proteins in this compartment (Kuismanen and Saraste, 1989; Jackson et al., 1993). FP-17 and -22 localization to the IC was then investigated in the temperature-blocked cells after immunostaining for the IC marker, endoplasmic reticulum–Golgi intermediate compartment (ERGIC)–53/p58 (Saraste et al., 1987; Schweizer et al., 1988). As shown in Fig. 2 c, in cells kept at 37°C for 75 min after microinjection, FP-22 was mainly localized in the ER, although it also partially colocalized with ERGIC-53. After 3 h at 15°C, it concentrated in ERGIC-53–positive IC elements (Fig. 2 d). In contrast, FP-17 showed no detectable colocalization with ERGIC-53 either before (Fig. 2 a) or after (Fig. 2 b) the

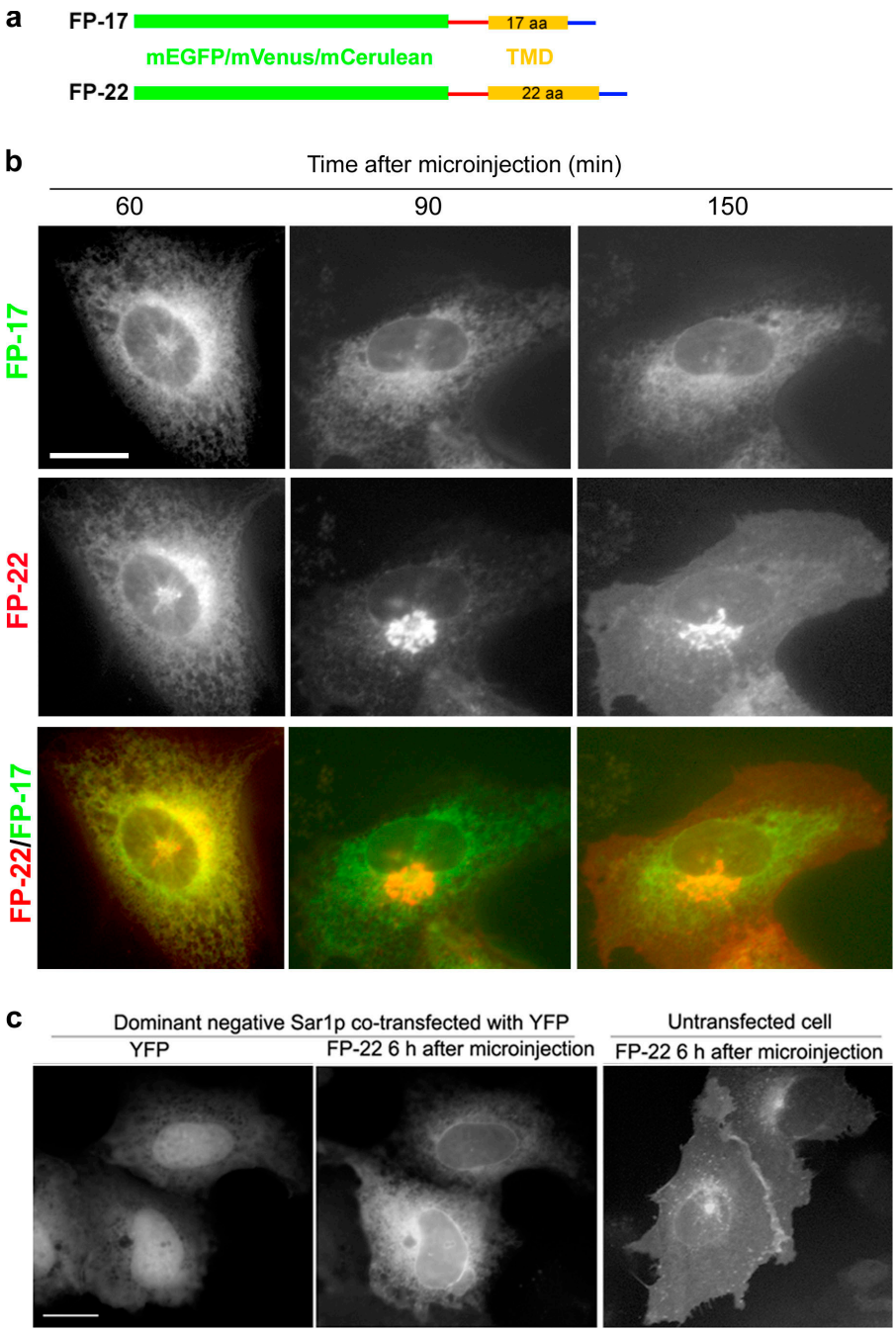

Figure 1. **After cDNA microinjection, FP-17 remains in the ER, wheras FP-22 is exported by a COPII mechanism and travels through the Golgi complex to the plasma membrane.** (a) Schematic representation of the two constructs. The N-terminal monomeric EGFP, Cerulean or Venus (green), are followed, in sequence, by the following: a linker (red) containing the myc epitope, a repeated Gly-Ser sequence, and residues 94–106 of rabbit cyt b5; the TMD (yellow) of cyt b5 (17 residues) or a modified version thereof extended by 5 residues (ILAAV); and the seven-residue C-terminal polar peptide (blue) of rabbit cyt b5. The N-terminal FP is exposed to the cytosol (Bulbarelli et al., 2002). (b) CV1 cells were microinjected with the cDNAs coding for Venus-17 and Cerulean-22 (left) or Cerulean-17 and Venus-22 (middle and right). 60 min after microinjection, 30 μg/ml cycloheximide was added. Cells were imaged alive by wide field microscopy for the two FPs at the indicated times after microinjection. The middle and right columns show the same cell, 30 (middle) and 90 (right) min after the addition of cycloheximide. In the bottom row, which shows the merged images for each time point, red and green pseudocolors are attributed to FP-22 and -17, respectively. (c) Exit of FP-22 from the ER is COPII-dependent. CV1 cells were cotransfected with H79G-Sar1 and YFP (as a marker of transfection; left) and 12 h thereafter microinjected with the cDNA coding for FP-22. Cells were fixed 6 h later and imaged by wide-field microscopy. 2D-deconvolved images are shown. The left and middle show the same field of microinjected cells visualized for YFP (left), and Cerulean-22 (middle), which remains in the ER in the H79G-Sar1–expressing cells. The right shows two microinjected cells that were negative for YFP and in which Cerulean-22 is at the cell surface. Bars, 10 μm.

temperature block, indicating that it does not have access to the IC under these conditions.

We then investigated whether FP-17 and -22 are recruited differently to ERES. 75 min after microinjection, cells were shifted to 10°C, a condition that blocks exit from the ER (Tartakoff, 1986; Lotti et al., 1996; Mezzacasa and Helenius, 2002). The cells were then analyzed for colocalization of the expressed FPs with endogenous COPII, revealed by immunostaining of the coat component Sec23. As shown in Fig. 3 a, both FP-17 and -22 appeared dispersed in the ER after incubation at reduced temperature. Nevertheless, examination at higher magnification revealed that FP-17 was often excluded from Sec23-positive puncta, whereas FP-22 was enriched in Sec23-positive puncta (Fig. 3 b). Quantitative analysis showed that after the 10°C block, the percentage of COPII puncta positive for FP-22 doubled, whereas FP-17 recruitment was unaffected (Fig. 3 c). Analysis of the Sec23 fluorescence after subtraction of the FP signal (see Materials and methods) confirmed a statistically significant difference in COPII colocalization of the two FPs after the 10°C block (Fig. 3 d).

As a positive control for recruitment of a transported membrane protein to ERES, we performed the same 10°C block experiment on cells microinjected with the GFP-tagged temperature-sensitive mutant (ts045) of vesicular stomatitis virus glycoprotein (VSVG; VSVG-GFP). In agreement with previously published results (Mezzacasa and Helenius, 2002), at the nonpermissive temperature for transport misfolded VSVG-GFP

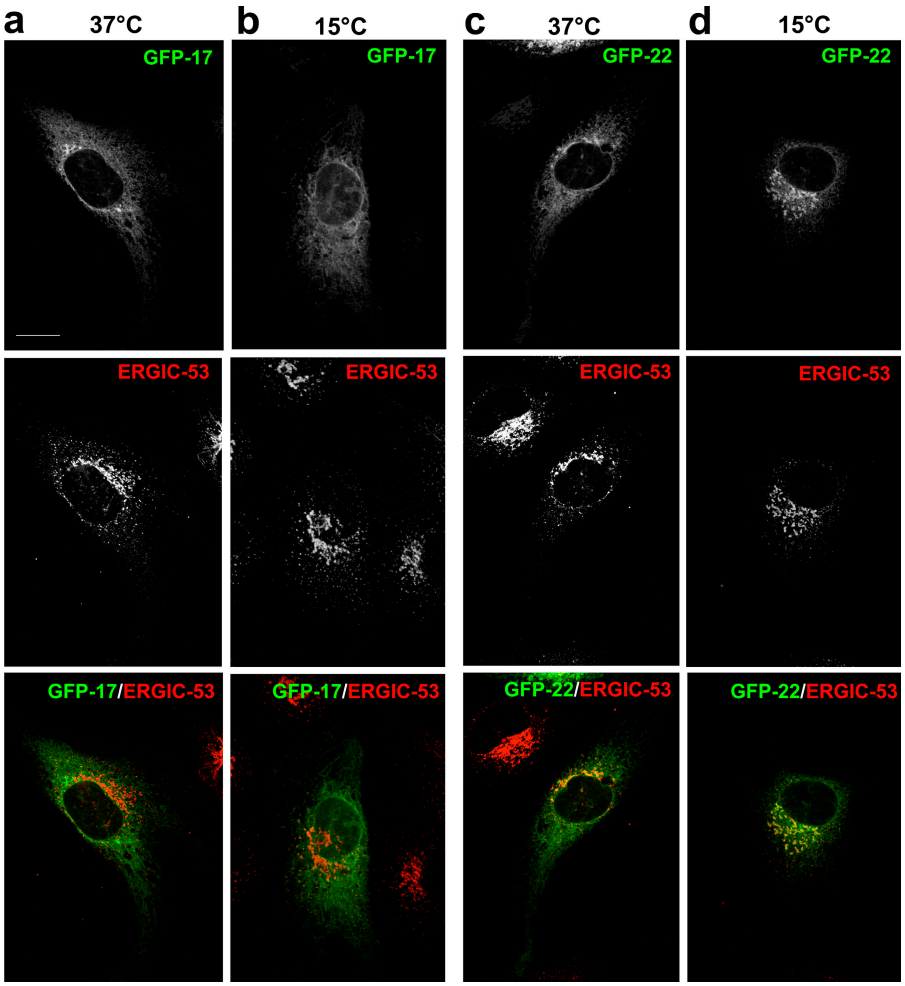

Figure 2. **Different effect of 15°C temperature block on FP-17 and -22 localization.** CV1 cells were microinjected with the cDNA coding for EGFP-17 or -22. After 75 min of incubation at 37°C (a and c), cells were fixed or further incubated at 15°C (b and d) for 3 h before fixation. The cells were immunostained for ERGIC-53, with the use of Alexa 568 secondary antibodies, and analyzed by confocal microscopy. Each column shows the same field visualized for GFP (top) or ERGIC-53 (middle), as well as the merged image with the indicated pseudocolors (bottom). Bar, 10 µm.

localized very poorly to ERES (Fig. 3 c). The subsequent low temperature incubation lead to recruitment of the viral protein to >70% of COPII-positive structures, compared with ∼35% in the case of FP-22 (Fig. 3 c). Subtraction analysis confirmed that VSVG-GFP colocalized with COPII better than FP-22 did after the temperature block (Fig. 3 d). Thus, the viral glycoprotein is recruited to ERES more efficiently than FP-22, presumably because of the diacidic export signal in its cytosolic tail (Nishimura and Balch, 1997).

Immunogold analysis of TMD-dependent sorting at ERES

To investigate the different recruitment of FP-17 and -22 to ERES at higher resolution, we performed immunogold experiments on cryosections of transfected HeLa cells subjected to a 10°C block 12 h after transfection, a time at which approximately half of the FP-22 is in the ER, with the remaining protein in the Golgi or at the cell surface (Fig. 4 d). To identify ERES by labeling of endogenous components, we tested several antibodies and chose an antibody against Sec16 (Watson et al., 2006; Bhattacharyya and Glick, 2007) that yielded low levels of labeling but was highly specific for the ER (for the characterization of its specificity see Table S1, available at http://www.jcb.org/cgi/content/full/jcb.200710093/DC1). The anti-Sec16 antibody was visualized with secondary antibodies conjugated to 12-nm gold particles, whereas the FP constructs were visualized with GFP antibody and a secondary antibody conjugated to 18-nm gold particles (for a characterization of the labeling specificity of the anti-GFP antibody see Table S2). 18-nm gold particles were often seen clustered near the 12-nm particles in cells expressing FP-22 (Fig. 4 b) but not in cells expressing FP-17 (Fig. 4 a).

To perform a quantitative analysis of the micrographs, we considered portions of ER continuous with an anti-Sec16–labeled membrane and within 60 nm of the 12-nm gold particle as ERES. In this unbiased analysis, morphology was not a criterion for the definition of an ERES (Fig. 4, c–g; for details see Materials and methods and Table S3, available at http://www.jcb.org/cgi/content/full/jcb.200710093/DC1). The results of this analysis indicated that FP-22 and -17 were significantly more and less concentrated, respectively, in ERES than expected on the basis of a random distribution within the ER (Fig. 4 g). Thus, the TMD-dependent sorting process operates both by exclusion of the short TMD and by weak recruitment of the long TMD bearing protein to ERES.

FP-22 and VSVG travel out of the ER in the same carriers

As shown in Fig. 5, when cells were coinjected with FP-22 and VSVG-YFP and kept at the permissive temperature for VSVG,

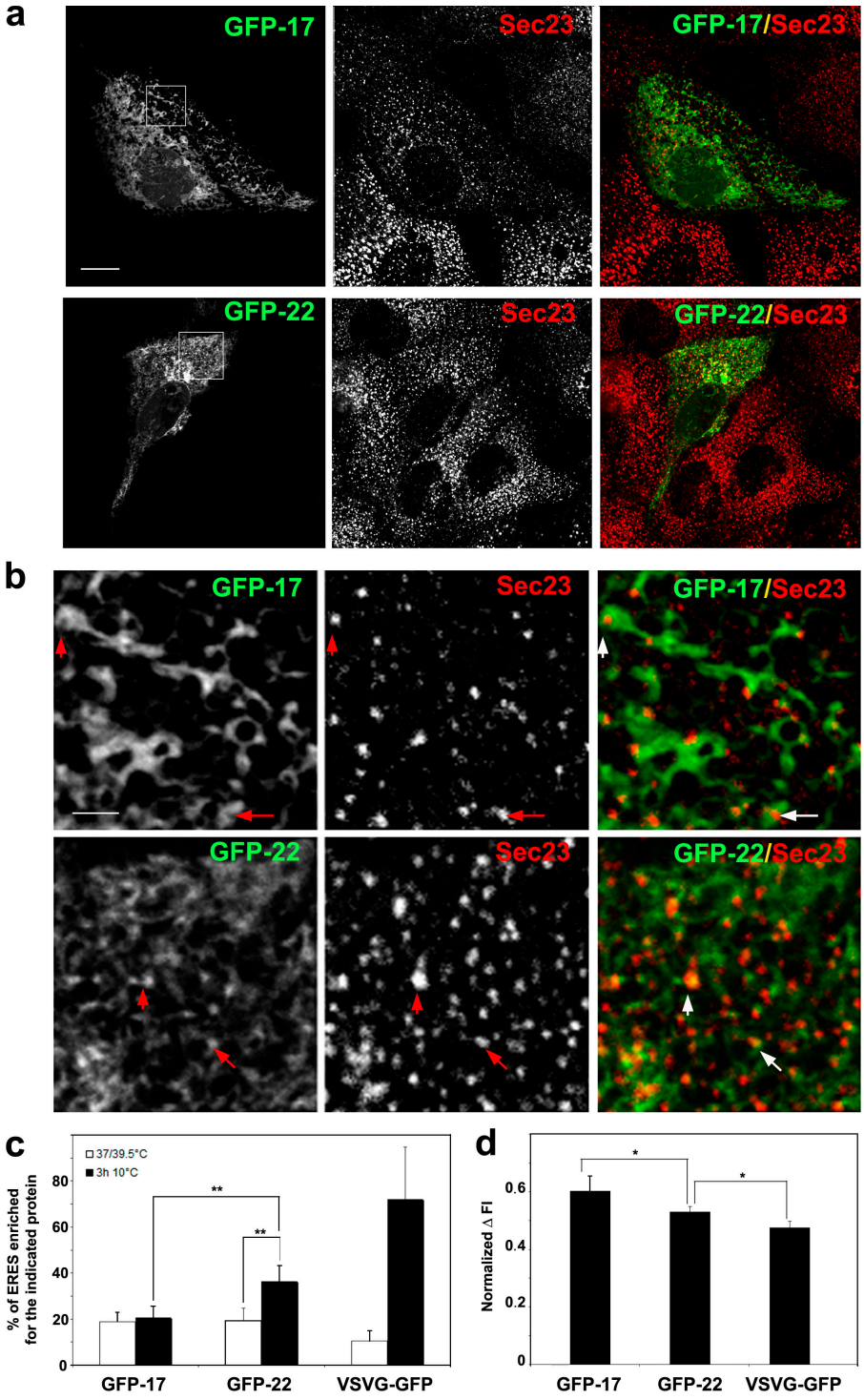

Figure 3. **Different accumulation of FP-17 and -22 at ERES after a 10°C temperature block.** (a and b) CV1 cells were microinjected with the cDNA coding for EGFP-17 or -22, incubated for 75 min at 37°C, and then at 10°C for 3 h. The cells were then fixed and immunostained for Sec23 with an Alexa 568–conjugated secondary antibody. Each row shows the same field visualized for GFP (left) or Sec23 (middle), as well as the merged image with the indicated pseudocolors (right). b shows enlargements of the boxed areas in a. Arrows in b indicate Sec23-positive puncta from which FP-17 appears excluded or in which FP-22 appears concentrated. Bars: (a) 10 μm; (b) 2 μm. (c) Percentage of Sec23-positive structures enriched in FP-17, FP-22, or VSVG-GFP before and after the 10°C temperature block. The analysis was performed on cells like the ones illustrated in a and b. Averages + SD are shown (FP-17 37°C, $n = 9$ cells; FP-17 10°C, $n = 12$ cells; FP-22 37°C, $n = 7$ cells; FP-22 10°C, $n = 12$ cells; VSVG 39°C, $n = 7$ cells; VSVG 10°C, $n = 6$ cells). White and black columns refer, respectively to cells kept at 37 (FP-17 and -22) or 39°C (VSVG-GFP) for 75 min after microinjection and to cells incubated for a further 3 h at 10°C. The values were determined by manual counting (see Materials and methods). **, $P < 0.0001$ (determined by one way analysis of variance followed by Fischer's protected least square difference analysis). (d) Subtraction analysis of cells after the 10°C block. FI of Sec23 was determined after subtraction of the fluorescence of the indicated protein. Normalized ΔFI is the ratio of the mean intensities of the subtracted to the unsubtracted image (see Materials and methods). A lower normalized ΔFI indicates a higher degree of colocalization. Means + SD are shown (FP-17, $n = 16$; FP-22, $n = 13$; VSVG, $n = 9$). *, $P < 0.05$ (for the difference between FP-22 and FP-17 and between FP-22 and VSVG, determined by the Kruskal-Wallis nonparametric test followed by Dunn's post-analysis.

the viral glycoprotein was never visualized in the ER, and was transported more rapidly to the plasma membrane than FP-22. We asked whether the different rate of transport of VSVG and FP-22 could be explained entirely on the basis of their different efficiency of recruitment to ERES (Fig. 3) or whether differences in transport rate occur also after budding of transport carriers.

When cells coinjected with Cerulean-22 and VSVG-YFP were blocked at 10°C, nearly all COPII-positive structures that contained Cerulean-22 were also positive for VSVG, indicating that the two proteins are recruited to the same ERES (Fig. 6, a and c). To follow the subsequent export step, the block was released on the microscope stage and cells were imaged during recovery. An example of a moving structure positive for both proteins is illustrated in Fig. 6 b. A quantitative analysis of similar time-lapse series is illustrated in Fig. 6 (d and e), where the spatial and temporal origins are defined as the position and last time point at which no movement of the considered structure was detectable. During a 1-min time interval, in which the mean displacement of the analyzed carriers was 3 μm (Fig. 6 d), the fluorescence intensity (FI) of both fluorophores was unaltered

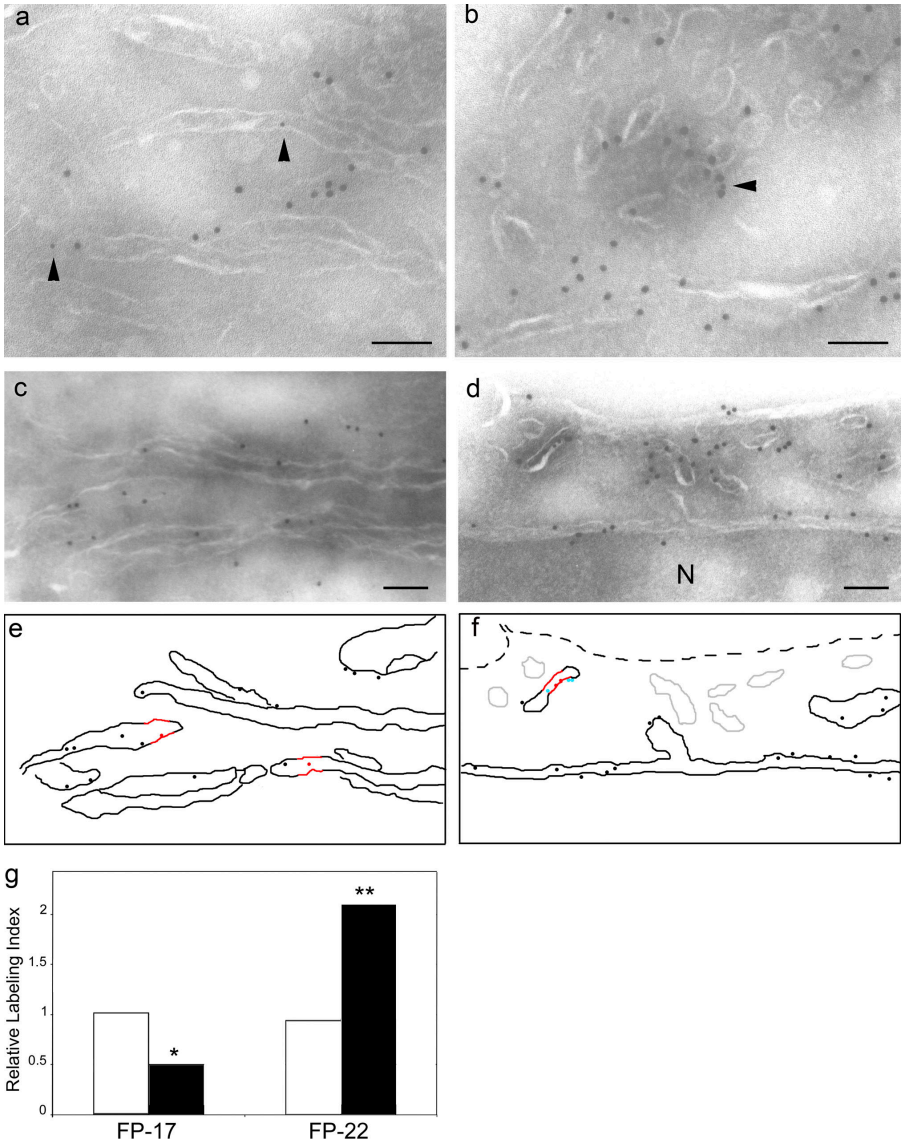

Figure 4. **Immunogold electron microscopy analysis of FP-17 and -22 distribution in the ER and ERES after the 10°C block.** (a–f) HeLa cells transfected with Venus-17 (a and c) or -22 (b and d) and incubated for 3 h at 10°C were processed for cryosectioning as described in Materials and methods. FPs and the ERES marker Sec16 are labeled with 18- and 12-nm gold particles, respectively. Arrowheads in a and c indicate 12-nm gold particles, which are in close proximity to 18-nm gold particles in the case of cells expressing FP-22 (b) but not FP-17 (a). c–f show two examples of how image analysis was performed. Starting from the images in c and d, we manually reconstructed the drawings in e and f, attributing unequivocally identifiable membrane profiles to ER (black) and, among these, membranes within 60 nm of a 12-nm gold particle to ERES (in red). Other intracellular membranes (not considered) are represented in gray. The dashed line in f represents the plasma membrane. Note that, as expected, in these transfected cells FP-22 is present also at the plasma membrane. Gold particles falling within 20 nm of ER (or ERES) and considered in the analysis are color-coded as follows: 12-nm gold particles used to identify ERES, red; 18-nm gold particles attributed to ER or to ERES, black and cyan, respectively. Bars, 100 nm. (g) Relative labeling index for FP-17 and -22 at the ER (white) and ERES (black). The analysis, performed on 25 and 19 micrographs for FP-17 and -22, respectively, demonstrates that neither of the two FP constructs is randomly distributed between ER and ERES, but although FP-17 is excluded from ERES, FP-22 is concentrated therein. Statistical significance was assessed by a test for randomness, modified from Mayhew et al., (2003; *, P = 0.044; **, P = 0.0007). For details, see Materials and methods and Tables S1–3, available at http://www.jcb.org/cgi/content/full/jcb.200710093/DC1.

with respect to the signal at the origin (Fig. 6 e), indicating that the two proteins accumulate at functional ERES and then travel out of the ER together. The relatively slow movement of the transport carriers compared with previous reports in the literature (Presley et al., 1997; Scales et al., 1997) is presumably caused by the low temperature at which we performed our observations. Thus, FP-22 accumulates at the same ERES as VSVG and its inefficient accumulation at these sites can account for its slower exit from the ER. Whether it is recruited with similar low efficiency into transport carriers at subsequent steps of the secretory pathway remains to be established.

At 37°C, FP-17 and -22 partition into different ER domains

Although FP-17 and -22 appear to colocalize in the ER at early times after microinjection (Fig. 1), closer inspection revealed that they occupy different domains within the organelle. When cells expressing FP-17 and -22 were examined by confocal microscopy 75 min after microinjection, a clear difference in their localization within the ER could be observed (Fig. 7 c). More specifically, FP-17 was found both in tubular and cisternal elements, whereas FP-22 was excluded from peripheral sheets (Fig. 7, enlargements in the three bottom rows), although it did localize to the perinuclear cisterna (Fig. 7 c). The different distribution of the two proteins was not caused by the attached FP variant because when the two variants (Cerulean and Venus) of each construct with the same TMD were expressed together, excellent colocalization was observed (Fig. 7, a and b) and because the same difference in localization of FP-17 and -22 was observed when the opposite combination of FP spectral variants was used (Fig. S1, available at http://www.jcb.org/cgi/content/full/jcb.200710093/DC1). Segregation between the two constructs was also observed at longer times after expression if export was inhibited by the dominant-negative mutant of Sar1p (unpublished data).

A recent study demonstrated that reticulon (Rtn) proteins induce ER tubule formation and are excluded from cisternal elements (Voeltz et al., 2006). We therefore compared the distribution of the two constructs with that of Rtn4a. As shown in Fig. 8, Rtn4a was restricted to the edges of ER elements filled with

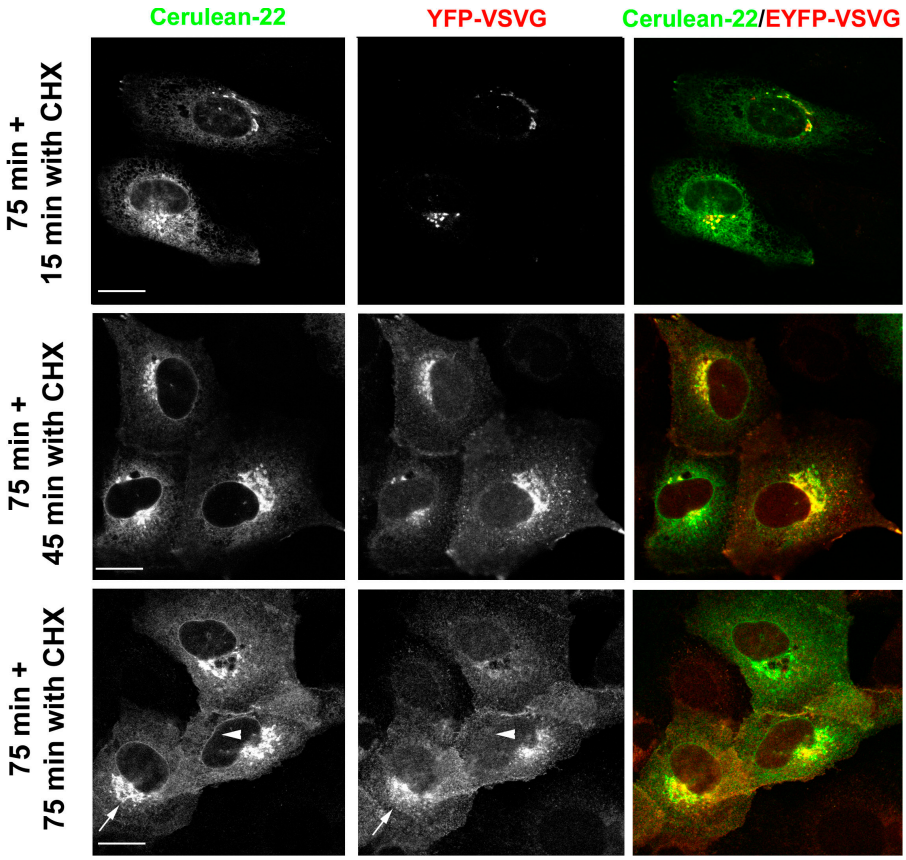

Figure 5. **Different rate of transport of FP-22 and VSVG to the plasma membrane.** CV1 cells, microinjected with the cDNA coding for Cerulean-22 and VSVG-YFP, were incubated for 75 min at 30°C and then at the same temperature in the presence of 50 μg/ml cycloheximide for the indicated times. Each row shows the same field visualized for the indicated protein as well as the merged image with the indicated pseudocolors. Even at the early time points, most of the viral protein is in the Golgi complex, whereas FP-22 is mainly in the ER. 45 min after cycloheximide addition, both the proteins are found in the Golgi and at the plasma membrane, although FP-22 is still present in the ER. At 75 min, although YFP-VSVG is almost totally localized at the plasma membrane, FP-22 is still found in the Golgi (arrows) and in the ER. Note that the nuclear envelope is visible in the cerulean (FP-22) but not the YFP channel (arrowheads). Bars, 20 μm.

FP-17 (left) but was present on FP-22–positive tubules (right). Thus, the construct with the longer TMD preferentially partitions into curved domains within the peripheral ER. Surprisingly, however, and at variance with the Rtns (Voeltz et al., 2006), FP-22 was not excluded from the perinuclear cisterna, reflecting structural/compositional differences between perinuclear and peripheral sheets that remain to be characterized.

FP-22 is freely diffusible within the ER and at ERES

Based on sucrose gradient and FRAP analysis, our previous work (Pedrazzini et al., 2000; Snapp et al., 2003b) indicated that cyt b5 and GFP-17 are freely diffusible in the ER, excluding the possibility that immobilization is responsible for its retention. On the other hand, export of many proteins requires oligomerization (for review see Lee et al., 2004). Therefore, we considered the possibility that the different distribution of the two FP constructs within the ER and at ERES could be caused by a higher propensity of FP-22 to form oligomers.

We first compared the mobility of FP-17, FP-22, and VSVG by the FRAP technique after a 75-min incubation of the microinjected cells at 39°C (Fig. 9 a). FP-17 displayed a high mobile fraction (M_f) and the same diffusion coefficient (D) as found in transfected cells in our previous work (Snapp et al., 2003b) with the same construct (called GFP-b(5)tail in that study), confirming its high mobility within the ER membrane. VSVG was also freely diffusible, although its D was somewhat lower than the one previously calculated by Nehls et al., (2000) with the use of a different procedure. Finally, FP-22 displayed an even higher D than FP-17, possibly reflecting its restriction to tubular elements.

Because the FRAP technique would not distinguish small oligomers from monomers, we also compared the sedimentation of FP-17 and -22 in detergent-solubilized cell lysates on sucrose gradients (Fig. 9b). As a control, we analyzed the distribution of endogenous ribophorin I, a protein known to be part of large complexes in the ER (Nikonov et al., 2002). Indeed, ribophorin (M_r ~68,000) was partly recovered in complexes running ahead of the catalase marker (M_r 240,000) as well as in the pellet. In contrast, both FP-17 and -22 showed a sharp peak in fraction 3, ahead of the cyt c marker (M_r 12,000) but well behind catalase, as expected on the basis of their monomeric M_r of ~34,000. Thus, two methods failed to reveal differences in the state of aggregation of FP-17 and -22.

To further investigate the dynamics of FP-22 partitioning in the ER, we analyzed its recovery after bleaching at single exit sites, comparing it with VSVG. Cells were microinjected with the cDNA coding for either of the two cerulean-tagged proteins, together with YFP-tagged Sec23 cDNA, to identify ERES. After incubation for 3 h at 10°C, the cells were kept at the same temperature on the microscope stage, and small areas encompassing single ERES were subjected to FRAP analysis. The examples of Fig. 10 (a and b) illustrate how FP-22 fluorescence recovered quite rapidly at ERES (b) in contrast to VSVG, which exhibited a low recovery over the time period analyzed (a). The mean time course of recovery in multiple ERES (Fig. 10 c) clearly revealed the different behavior of the two proteins. Whereas FP-22 FI in the bleached ERES rapidly reached a plateau value of

Figure 6. **Analysis of FP-22 and VSVG-YFP during export from the same ERES.** (a) Imaging of fixed cells. CV1 cells, microinjected with the cDNAs coding for Cerulean-22 and VSVG-Venus, were incubated for 75 min at 39.5°C and then for 3 h at 10°C before fixation. Cells were immunostained for Sec23, using Cy5-conjugated secondary antibodies, and analyzed by confocal microscopy. Single-channel images for the three proteins, and a merged image with the indicated pseudocolors are shown. The arrowheads indicate Sec23-positive structures containing both FP-22 and VSVG. The arrows indicate a structure positive for Sec23 and VSVG but lacking Cerulean-22. Bar, 10 µm. (b) Time-lapse imaging of carriers leaving the ER with VSVG and FP-22 cargo. Cells were microinjected, incubated as described in a, and then imaged while warming to 20°C (see Materials and methods). Each column shows images of the same field at the indicated times after the start of imaging in the Cerulean and YFP channels, as well as the merge of the two channels (bottom) with the indicated pseudocolors. Arrowheads indicate a moving carrier and open circles in the merge indicate the initial position of the structure. Bar, 5 µm. (c) Results of quantification of images like the one in a. The percentage of ERES positive for the indicated protein is shown. Numbers are means ± SD (n = 6). (d) Mean displacement versus time of moving carriers. Initiation of movement at different ERES was not synchronous, and the 0 time point corresponds to the last image before initiation of movement for each carrier. For each carrier at each time point, the displacement was calculated as the sum of displacements occurring during all preceding time intervals. Shown are means ± SD. (e) FI in the Cerulean and YFP channels of moving carriers normalized to the FI at their origin. Carriers in each of seven images were classified according to displacement from the origin within the distance intervals indicated on the abscissa. Means ± SD are shown. The data in d and e were acquired from the analysis of five cells.

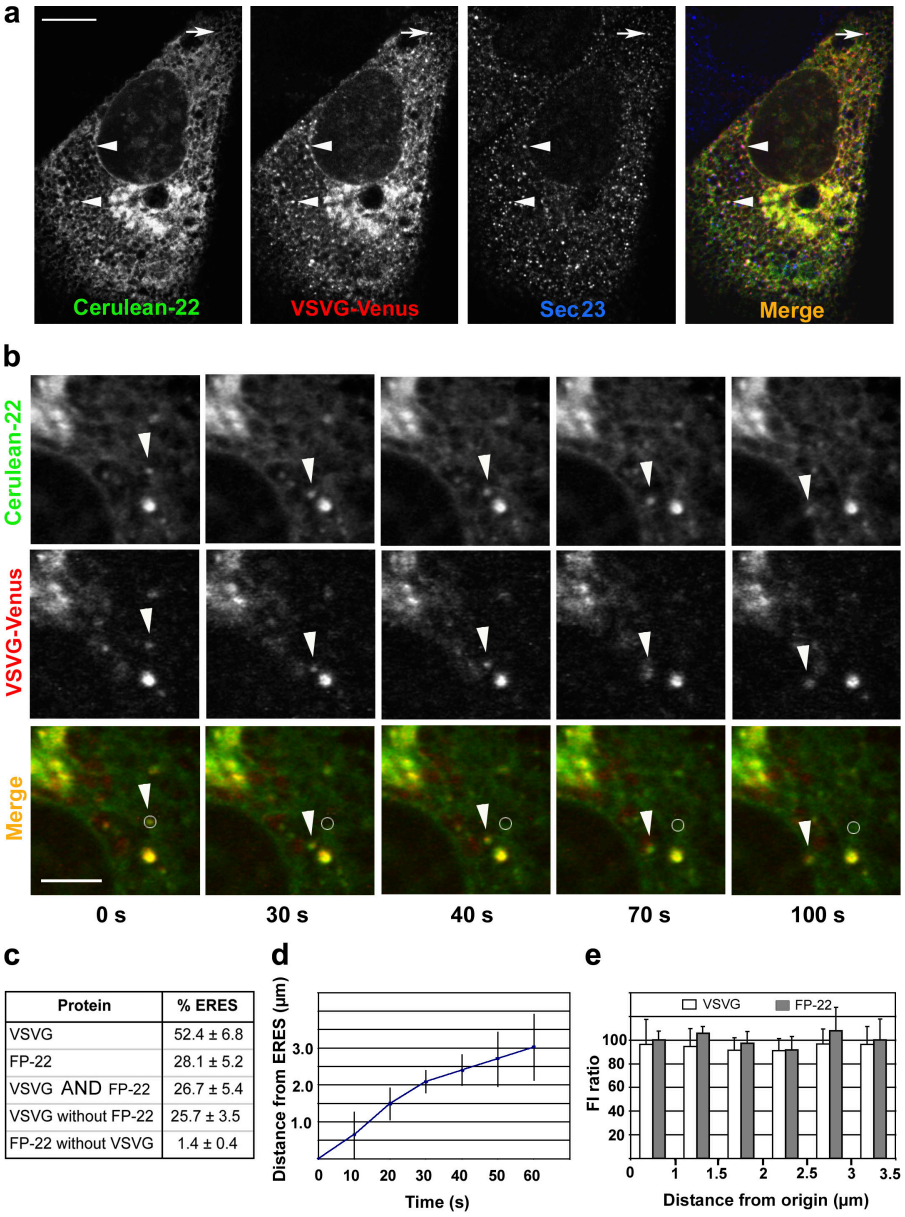

c

Protein	% ERES
VSVG	52.4 ± 6.8
FP-22	28.1 ± 5.2
VSVG AND FP-22	26.7 ± 5.4
VSVG without FP-22	25.7 ± 3.5
FP-22 without VSVG	1.4 ± 0.4

90% of the prebleach intensity, VSVG slowly increased during the entire recovery period. The latter finding might be explained in part by the much lower amount of surrounding ER as source of fluorescent VSVG molecules diffusing into the ERES and is also compatible with the idea that VSVG is restricted at ERES by interacting with limiting binding sites.

We also compared the recovery kinetics of FP-22 at ERES with its recovery in the ER outside of exit sites. To do this, cells, microinjected with cDNA for Sec23-YFP and FP-22 and incubated at 10°C as in the previous paragraph, were subjected to bleaching over a 2.4-µm strip encompassing the entire width of the cell and containing at least one ERES. Recoveries in the entire strip and in the ERES within it were then compared. The extent and rate of recovery of FP-22 within the bulk ER and into exit sites were similar (Fig. 10 d). The rapid attainment in ERES of prebleach values (which were at least twice those of the surrounding ER) cannot be explained merely by recovery into the bulk ER contained in the optical sections above and below the exit sites and supports the idea that transient interactions not involving saturable binding sites underlie the accumulation of FP-22 at ERES.

Discussion

The structure and function of ER subdomains and the dynamic relationship between them is currently a subject of intense investigation (Snapp et al., 2003b; Voeltz et al., 2006). In the present study, we demonstrate that TMD length/hydrophobicity can determine how a membrane protein partitions between ER tubular, cisternal, and exit site domains, suggesting a role for protein–lipid interactions in sorting phenomena both within the ER and between the ER and the Golgi complex.

Although there is detailed information on the retrieval phenomena that operate within the exo–endocytic pathway to

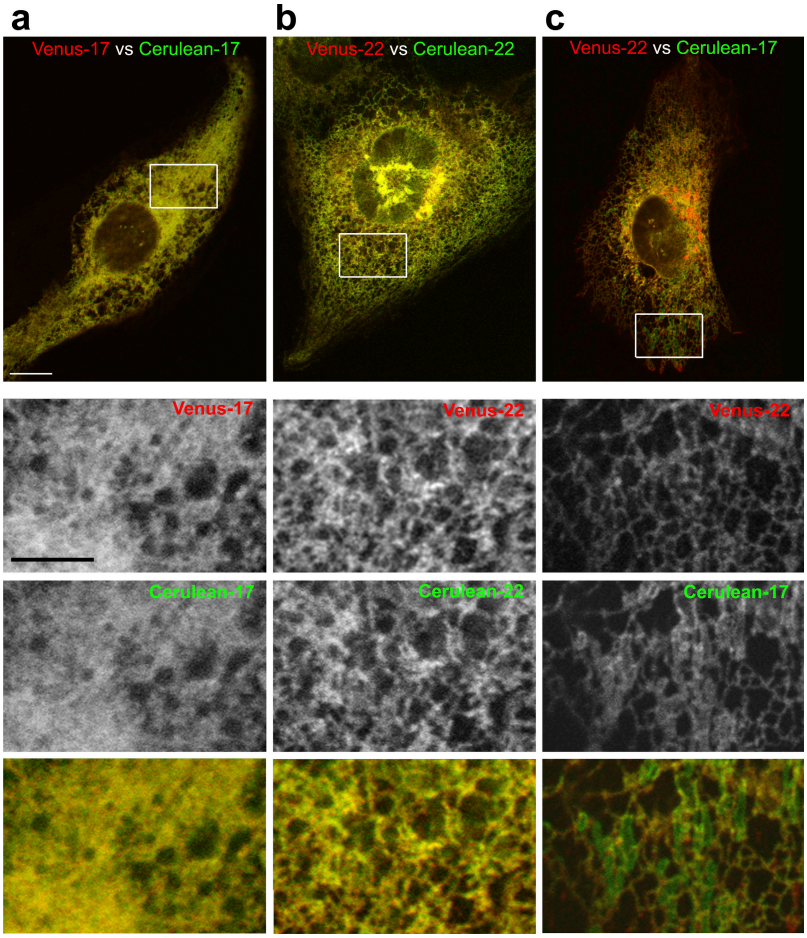

Figure 7. **FP-17 and -22 segregation within the ER.** Cells were microinjected with cDNAs coding for different couples of FPs, as indicated in the top, and fixed after 75 min at 37°C. The bottom three rows show single-channel and merged images, with the indicated pseudocolors, of enlargements of the boxed areas in the top. Note sheet-like structures in c containing FP-17, from which FP-22 is excluded. Bars: (top) 10 μm; (enlargements) 5 μm.

counteract escape of proteins from their compartment of residence (for reviews see Bonifacino and Glick, 2004; Lee et al., 2004), it has been more difficult both to demonstrate and to elucidate the static retention mechanisms that underlie exclusion of resident proteins from transport carriers. Cell-free budding assays have provided a powerful tool to investigate the role of export signals in cargo packaging (for reviews see Bonifacino and Glick, 2004; Lee et al., 2004), but their low efficiency limits their usefulness in distinguishing weak recruitment into transport carriers from outright exclusion. In in vivo approaches, failure of a protein to accumulate in ERGIC-53–positive elements after a 15°C temperature block was often taken as evidence for its static retention (Pentcheva et al., 2002; Schamel et al., 2003). However, recycling through early IC elements might not be easily discernable and could be insensitive to the temperature block, as suggested by undetected accumulation of some recycling proteins in ERGIC-53–positive elements (Jackson et al., 1993; Stornaiuolo et al., 2003).

In this paper, to elucidate the mechanism of TMD-dependent sorting at the ER–Golgi interface, we have overcome these limitations by directly comparing the recruitment of our two model TA proteins to ERES, the ER subdomains where anterograde transport carriers are generated (Watson and Stephens, 2005). By immunofluorescence, a 10°C temperature block resulted in the recruitment of FP-22 to ERES, whereas FP-17's localization to these sites remained low. High resolution quantitative immunogold analysis confirmed that FP-22 undergoes mild accumulation at ERES after the temperature block, whereas FP-17 is at least partially excluded from these sites. Furthermore, FP-17 and -22 were partially segregated within the ER in the absence of any temperature block. Although FP-17 was present both in tubules and sheets, FP-22 was clearly excluded from peripheral sheets and restricted to Rtn4a-positive tubules and to the nuclear envelope.

The TMD-dependent sorting reported here is difficult to reconcile with a receptor-mediated mechanism (see also the considerations in the Introduction). It has been suggested that resident proteins are excluded from ERES by receptor-independent mechanisms simply because they are not recognized by the export machinery (Pentcheva et al., 2002). However, this idea is at variance with recognized bulk flow phenomena (Martinez-Menarguez et al., 1999) and with the observation that removal of identified export signals usually causes slowdown but not complete block of the modified protein's export (Fiedler et al., 1996; Nishimura and Balch, 1997; Iodice et al., 2001). Thus, we postulate that a positive but receptor-independent mechanism underlies the exclusion of FP-17 from ERES. Such a mechanism could, in principle, rely on immobilization within a protein matrix (Hammond and Helenius, 1995) or on partitioning phenomena that would drive FP-17 into membrane domains excluded from budding transport carriers (Ceppi et al., 2005). The high diffusion coefficient of FP-17, determined by FRAP

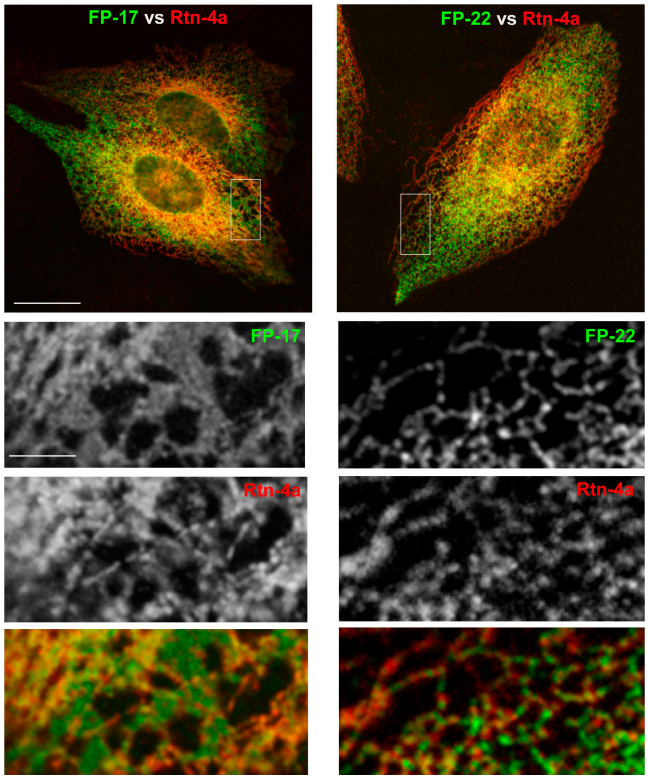

Figure 8. **Rtn4a is excluded from FP-17–positive ER cisternae.** Cells were microinjected with cDNAs coding for EGFP-17 or -22 (both lacking the myc epitope in the linker region) and myc-tagged Rtn4a, as indicated in the top. Cells were fixed after 75 min at 37°C, and Rtn4a was revealed with an anti-myc monoclonal followed by secondary Alexa 568–conjugated antibodies. The bottom 3 rows show single-channel and merged images, with the indicated pseudocolors, of enlargements of the boxed areas in the top panels. Bars: (top) 20 µm; (enlargements) 4 µm.

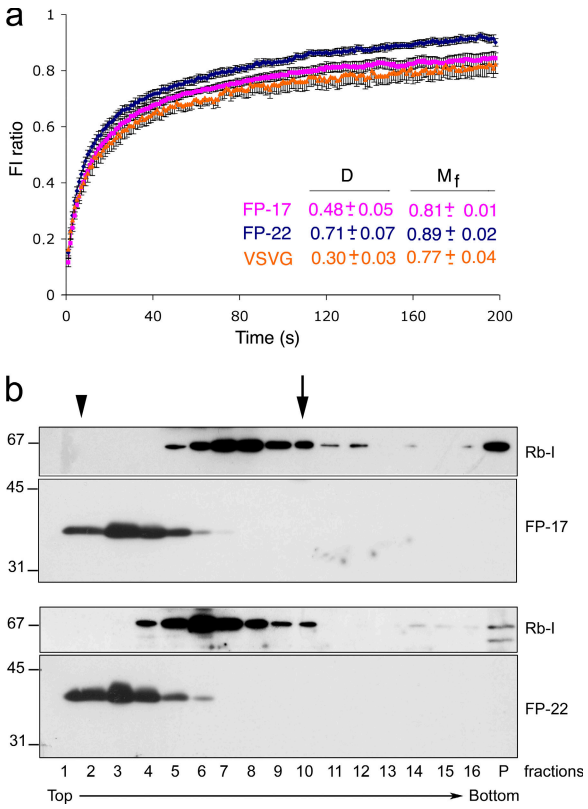

Figure 9. **State of aggregation of FP-17 and -22 investigated by two different methods.** (a) FRAP analysis of the two constructs in the ER. CV1 cells were microinjected with the cDNA coding for EGFP-17, EGFP-22, or VSVG-EGFP. FRAP experiments were performed after 75 min. Values in the ordinate are FI normalized to the prebleach value (see Materials and methods). Data points are means ± SEM for FP-17 (magenta; n = 11), FP-22 (blue; n = 10), and VSVG (orange; n = 6). The table gives the estimated D (in μm^2/sec) and M_f values ± SEM. Videos 1 and 2 (available at http://www.jcb.org/cgi/content/full/jcb.200710093/DC1) illustrate typical time-lapse series for FP-17 and -22, respectively. (b) Sucrose gradient analysis of postnuclear supernatants obtained from detergent-lysed CV1 cells 16 h after transfection either with EGFP-17 or -22 (see Materials and methods). Aliquots of the fractions were analyzed by SDS-PAGE followed by Western blotting for ribophorin I (Rb-I) or GFP, as indicated. The arrow and arrowhead indicate the position of cyt c and catalase, run on the gradients as size markers. P, pellet. Numbers on the left of the panels indicate position and M_r ($\times 10^{-3}$)of SDS-PAGE size markers.

analysis (Snapp et al., 2003b; this study), excludes the involvement of the first of these mechanisms and suggests that the second one underlies the TMD-dependent sorting reported here.

Reasoning in a similar way, it is difficult to explain the exclusion of freely diffusible FP-22 from ER-peripheral sheets on the basis of a receptor-mediated mechanism. Furthermore, the finding that, after bleaching, FP-22 fluorescence recovered at the same rate in ERES as in the bulk ER is compatible with a model positing that FP-22's accumulation in ERES is simply because of a lower exit rate than entry rate constant of the reporter construct and that no limiting binding site is involved in retaining it within these ER subdomains.

What physicochemical differences of the ER bilayer could justify the TMD-dependent partitioning observed in the present study? FP-22's TMD is more hydrophobic than FP-17's, and, if in α-helical conformation, is predicted to be longer than the thin hydrophobic core (~2.6 nm; for review see Sprong et al., 2001) of the ER membrane (positive mismatch). FP-22's TMD could thus seek ER subdomains in which the lipid composition better matches its length/hydrophobicity. Although detailed information is lacking so far, lipid compositional differences between ERES, transport carriers, and the bulk of the ER are very likely to exist. For instance, acidic phospholipids, namely phosphatidic acid and phosphtaidylinositol-4-phosphate play key roles in formation of COPII-coated carriers at ERES (Matsuoka et al., 1998; Pathre et al., 2003; Blumental-Perry et al., 2006), and phosphatidylserine with long saturated acyl chains accumulates in transport vesicles generated in vitro from microsomes (Sturbois-Balcerzak et al., 1999). Other compositional differences, for instance in sterols (Runz et al., 2006) and/or sphingolipids (Rosenwald et al., 1992; Muniz and Riezman, 2000), could contribute to a partitioning effect underlying the observed TMD-dependent sorting at ERES. In addition, the raft-like microdomains that have been suggested to exist in the ER (Bagnat et al., 2000; Muniz and Riezman, 2000; Lee et al., 2002; Browman et al., 2006; Campana et al., 2006; Smith et al., 2006) could be related to the partial segregation of the two proteins within this organelle.

Our previous results with a model system consisting of proteoliposomes reconstituted either with wild-type cyt b5 or cyt b5 with an extended TMD are fully consistent with the hypothesis of lipid-based sorting (Ceppi et al., 2005). Differential

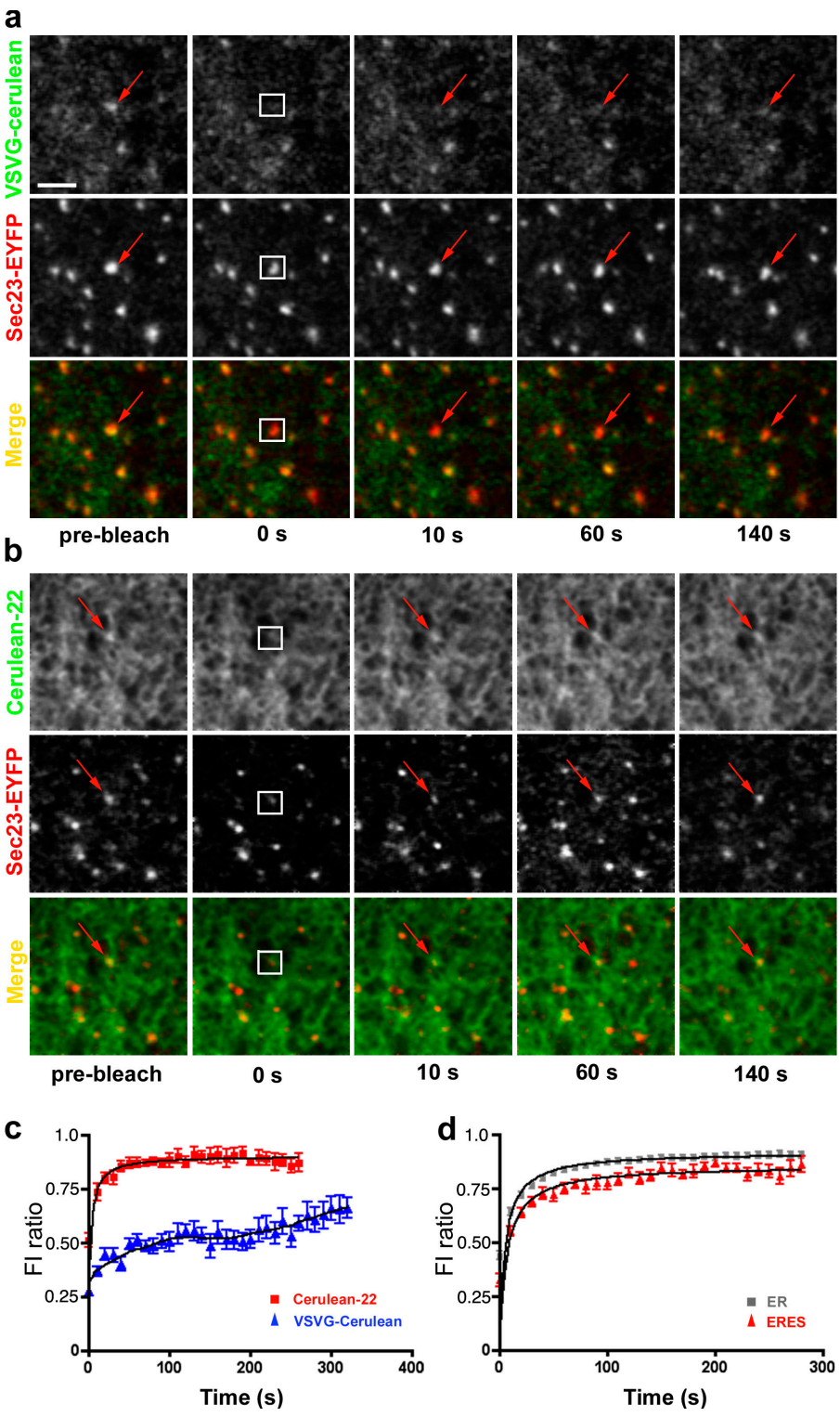

Figure 10. **FRAP analysis of FP-22 and VSVG at exit sites during a 10°C block.** (a and b) Bleaching of single ERES in cells doubly microinjected with Sec23-EYFP and VSVG-cerulean (a) or Cerulean-22 (b). 1.5 × 1.5-μm areas (indicated by the squares in the second column) encompassing single ERES (recognized by the presence of Sec23-EYFP; a and b, middle), were bleached for cerulean with the 456-nm line of the argon laser, and recovery into the ERES of the cerulean-tagged constructs was imaged at the indicated times. Each column shows the same field visualized for the indicated protein as well as the merged image with the indicated pseudocolors. The arrows indicate the ERES that was bleached and followed during recovery. Bar, 2 μm. (c) recovery curves for VSVG (blue) or FP-22 (red) containing ERES. (d) Comparison of recovery curves for FP-22 in the ER and in ERES after bleaching of a 2.4-μm strip (see Materials and methods). FP-22 recovers with a similar rate in ERES (red) and in the entire strip (gray). In c and d, values in the ordinate are FI normalized to the prebleach value (see Materials and methods). Shown are means of acquired data ± SEM (n = 10).

scanning calorimetry and fluorescence measurements of lipid probes revealed that the extended b5 mutant (which, in vivo, is sorted to the plasma membrane; Pedrazzini et al., 1996) partitions preferentially into domains enriched in acidic phospholipids or in ceramide and that the wild-type protein is partially excluded from these domains.

In addition to lipid composition, other physicochemical heterogeneities within the ER bilayer could contribute to the partitioning of FP-22's positively mismatched TMD. For instance, ER subdomains differing in thickness could be generated by differences in protein rather than in lipid composition (Mitra et al., 2004). Furthermore, simple geometrical considerations might explain the preferential partitioning of FP-22's TMD into ER tubules. One way of accommodating positive mismatch is by tilting of the TMD within the bilayer (for review see de Planque and Killian, 2003); however, this arrangement results in suboptimal

interaction between the TMD and the acyl chains, which are roughly perpendicular to the plane of the membrane. In curved domains some of the phospholipid hydrocarbon chains may be slightly tilted with respect to the bilayer perpendicular, generating microdomains in which the difference between the orientation of the acyl chains and of the TMD is smaller.

In conclusion, our results illustrate how relatively small differences in partitioning behavior can result in efficient sorting of membrane proteins. Indeed segregation of FP-22 from FP-17 was only partial. FP-22 was recruited weakly to exit sites, freely exchanging between them and the surrounding ER, and FP-17 was not completely excluded from ERES. The latter observation is consistent with our previous finding (Pedrazzini et al., 2000) that cyt b5 very slowly cycles between the ER and the Golgi. Thus, the difference in behavior of FP-17 and -22 in the early secretory pathway appears to be quantitative rather than qualitative, yet the cumulative effect of these quantitative differences is a qualitatively different final distribution of the two proteins. The TMD-dependent sorting based on partitioning described here, although observed with simple model transmembrane protein reporters, may be relevant to the mechanism by which the TMD influences the fate of more complex membrane proteins at the ER–Golgi boundary as well as at other sorting sites of the exo–endocytic pathway.

Materials and methods

Plasmids and antibodies

Constructs consisting of spectral variants of monomeric GFP linked at the C terminus to the TMD of cyt b5 (17 residues) or to an extended version thereof (22 residues) are called FP-17 and FP-22, respectively. Alternatively, they are referred to with the name of the spectral FP variant followed by the TMD length (Fig. 1 a). These constructs were generated from the previously described GFP-17 and -22 pCDNA3 plasmids (Bulbarelli et al., 2002) by replacing the GFP coding sequence with a monomeric EGFP variant (Snapp et al., 2003b) or with monomeric versions of Venus (F223R; Nagai et al., 2002) or Cerulean (A206K; Rizzo et al., 2004). Versions of EGFP-17 and -22 lacking the myc epitope in the linker between the FP and the TMD (Δmyc constructs; Bulbarelli et al., 2002) were used in colocalization experiments with myc-tagged Rtn4a. Other plasmids and antibodies used in this study are listed in Table S4 (available at http://www.jcb.org/cgi/content/full/jcb.200710093/DC1).

Transfection, microinjection, and temperature block experiments

CV1 and HeLa cells were transiently transfected by the calcium phosphate method or with the Fugene 6 reagent (Roche) as previously described (Bulbarelli et al., 2002). Plasmids were microinjected into the nucleus of CV1 cells with a microinjector (Eppendorf 5200), applying a pressure of 80–90 hPa. At the times indicated in the figure legends, microinjected cells were either imaged alive or fixed in 4% PFA. For temperature block experiments, cells were incubated in a refrigerated circulating water bath in Hepes-containing DME before fixation or live cell imaging.

Fluorescence microscopy

Imaging of fluorescent cells was performed with an MRC 1024 ES (Bio-Rad Laboratories) or an LSM 510 Meta confocal microscope (Carl Zeiss, Inc.), using 60× (Nikon) or 63× (Carl Zeiss, Inc.) Plan Apochromat lenses (1.4 NA), respectively. Unless otherwise specified, single confocal sections are shown in the figures. In some experiments, we used a wide-field microscope (Axiovert 200; Carl Zeiss, Inc.; 63× Plan Apochromat lens) equipped with a charge-coupled device camera (MicroMAX 512 BFT; Princeton Instruments) and controlled by Metamorph software (Crisel Instruments). For live-cell imaging, cells were kept in an on-stage thermostated and humidified CO_2 incubator.

In all cases, illustrations were prepared with Photoshop software (Adobe). Gamma adjustment was applied where required for easier visualization. Some of the images acquired by wide-field microscopy were deconvolved with the use of Huygens software (SVI; figure legends).

PFA-fixed cells were processed for immunofluorescence as previously described (Bulbarelli et al., 2002), except for Sec23 immunostaining. In the latter case, cells were permeabilized with 0.1% saponin in the presence of 50 µg/ml RNase A, a treatment that reduced nonspecific nuclear staining. Immunostained preparations were mounted in Vectashield (Vector Laboratories) or Mowiol (Sigma-Aldrich).

Colocalization analysis. To evaluate the extent of colocalization between expressed fluorescent constructs and endogenous COPII (visualized by Sec23 staining of fixed cells), two different methods were used. In the first, the percentage of colocalization was quantified by manual counting. First we applied a threshold to the Sec23 signal corresponding to seven times the mean FI of the entire cell, and the number of puncta within the size range of 4–50 pixels was quantified with the ImageJ program (Nation Institutes of Health). We then examined each Sec23-positive structure in the FP channel and scored a positive count when we found an enrichment of the FP fluorescent signal covering >50% of the thresholded pixels of Sec23. Differences between the percentage of COPII-positive structures containing FP-17 or -22 at 10 or 37°C were then evaluated by one-way analysis of variance, after transformation of the data to obtain a normal distribution, according to the equation $p' = \arcsin \sqrt{p}$ (where p is the observed percentage and p′ is the transformed value). Diverging groups were identified by Fischer's protected least square difference analysis.

In the second method, the degree of colocalization between different fluorescent constructs and Sec23 was compared by image subtraction. Images were acquired with laser power and gain adjusted so as to obtain similar mean intensities in the Sec23 and FP channels, and then processed and analyzed with the ImageJ program. After excluding the nucleus and the Golgi area and after background subtraction, the mean intensities were equalized in the two channels by reducing the upper limit of the display range of the dimmer of the two images. Finally, the FP signal was subtracted from that of Sec23, and the integrated FI of the subtracted image (ΔFI) was determined. Statistical significance of the ΔFI for the three groups of cells (expressing FP-17, FP-22, or VSVG) was assessed by the Kruskal-Wallis nonparametric test followed by Dunn's multiple comparison test.

To assess the degree of colocalization between FP-22 and VSVG at ERES, cells were doubly microinjected with Cerulean-22 and VSVG-YFP. After immunostaining the 10°C-blocked cells for Sec23, the same manual counting method was applied as described for singly microinjected cells.

To compare export of VSVG and FP-22 from the ER, cells coinjected with the cDNAs for VSVG-YFP and Cerluean-22 and blocked at 10°C were allowed to warm to 20°C in the on-stage incubator and imaged during warm-up. FI in the Cerulean and YFP channel was determined at ERES and in moving structures generated from there at 10-s time intervals, with the pinhole set at three times the value of the Airy disk.

Immunoelectron microscopy

Sample preparation. 12 h after transfection with Venus-17 or -22, HeLa cells were incubated at 10°C for 3 h. Glutaraldehyde and PFA were then added to the culture medium to final concentrations of 0.1% and 2%, respectively. Fixation was for 20 min at 10°C followed by 2 h at room temperature. The cells were then processed according to standard procedures (Griffiths et al., 1984). Cryosections were doubly labeled with rabbit polyclonal anti-GFP and sheep polyclonal anti-Sec16 antibodies, followed by secondary antibodies conjugated to 18- and 12-nm colloidal gold, respectively. Immunolabeled sections were stained and embedded in a mixture of methylcellulose: saturated uranyl acetate (9:1; Griffiths et al., 1984).

Colocalization analysis. The degree of localization of FPs to ERES on doubly immunodecorated cryosections was determined on images with a final magnification of 71,250 or 97,500. Only gold particles that fell within 20 nm of the ER membrane were taken into account. Membrane profiles were considered as ER if they were part of the nuclear envelope or of elongated tubular/cisternal structures (with a major diameter of at least 0.2 µm) or if they were labeled by at least one 12-nm gold particle (Sec16). We considered as ERES portions of ER membrane within 60 nm of, and in continuity with, a 12-nm gold particle–labeled site. In some micrographs, the 12-nm gold particle fell in the ER lumen so that it was not possible to determine from which of the two opposing membranes the signal originated. Therefore, we always considered both of the two opposing membranes of the ER region surrounding a 12-nm gold particle (Fig. 4 f).

Statistical analysis. The immunoelectron microscopy data were analyzed with a test for randomness (Mayhew et al., 2003), applied either to evaluate the specificity of the immunolabeling procedure or modified to

consider only the distribution of gold particles between ER and ERES (Tables S1–3). χ^2 values, calculated from the difference between observed and expected gold particles, were used to assess statistical significance.

FRAP

FRAP was performed on microinjected cells expressing EGFP-17, EGFP-22, or VSVG-EGFP, with the use of a confocal microscope (LSM 510 Meta). To compare D values of the three proteins within the ER, bleaching was performed on cells incubated at 39.5°C for 75 min after the microinjection. Experiments aimed at analyzing the dynamics of the FPs at single exit sites were conducted at 10°C on 10°C-blocked cells.

Evaluation of diffusion coefficients at 39.5°C. After two prebleach acquisitions, a 3.8-µm-wide strip across the entire width of the cell was scanned 50 times with the 488-nm line of the Argon laser at 100% power with the pinhole wide open. Recovery in the photobleached area was then followed at 1-s intervals for 200 s with attenuated laser power and with open pinhole. D and M_f values were estimated as previously described (Snapp et al., 2003a), applying the simulation method introduced by (Siggia et al., 2000).

FRAP at single exit sites. To identify ERES, cells were coinjected with a plasmid coding for Sec23-YFP together with the cDNA for the FP under investigation (VSVG-cerulean or Cerulean-22). A 1.5 × 1.5-µm area encompassing a single exit site was bleached with the 458-nm line of the Argon laser in the temperature-blocked cells, as described in the preceding paragraph, and recovery was followed with attenuated laser power in both the cerulean and the YFP channel with the pinhole set at a value of 5 Airy disks. The size of the area and the pinhole opening were chosen to avoid problems associated with possible small movements of the ERES during the experiment. In each image, recovery in the single ERES was computed after defining its position by comparison with the Sec23-YFP marker. To compare diffusion of FP-22 in ERES with that in the rest of the ER, cells, microinjected and blocked at 10°C, were strip bleached as described in the preceding paragraph. Recovery was then analyzed both in the ERES within the strip (identified by Sec23-YFP) and in the entire strip.

Sucrose density gradient velocity centrifugation

16 h after transfection with FP-17 or -22 cDNA, CV1 cells were lysed with detergent and analyzed by sucrose density gradient centrifugation as previously described (Pedrazzini et al., 2000).

Online supplemental material

Fig. S1 illustrates the segregation between Venus-17 and Cerulean-22. Tables S1 and 2 show the detailed morphometric analysis of the antibody specificity in Immunogold electron microscopy experiments. Table S3 reports the quantitative analysis of the distribution of FP-17 and -22 between ER and ERES by immunoelectron microscopy. Table S4 is a list of the plasmids and antibodies used in this study. Videos 1 and 2 show examples of FRAP experiments for FP-17 and -22, respectively. Online supplemental material is available at http://www.jcb.org/cgi/content/full/jcb.200710093/DC1.

In addition to the people who kindly supplied us with reagents and who are listed in Table S4, we thank Stefano Bonatti and Pietro De Camilli for critically reading the manuscript and Erik Snapp for assistance in determining diffusion coefficients by the FRAP technique. Special thanks to the Monzino Foundation (Milano, Italy) for its generous gift of the LSM 510 Meta confocal microscope.

This work was supported by an institutional Consiglio Nazionale Ricerche grant (ME.P02.007), by the Italian Ministry of Research (PRIN 2006 to N. Borgese), and by Telethon Foundation (grant N. GGP04129 to N. Borgese).

Submitted: 16 October 2007
Accepted: 14 March 2008

References

Aridor, M., S.I. Bannykh, T. Rowe, and W.E. Balch. 1995. Sequential coupling between COPII and COPI vesicle coats in endoplasmic reticulum to Golgi transport. *J. Cell Biol.* 131:875–893.

Bagnat, M., S. Keranen, A. Shevchenko, and K. Simons. 2000. Lipid rafts function in biosynthetic delivery of proteins to the cell surface in yeast. *Proc. Natl. Acad. Sci. USA.* 97:3254–3259.

Bhattacharyya, D., and B.S. Glick. 2007. Two mammalian Sec16 homologues have nonredundant functions in endoplasmic reticulum (ER) export and transitional ER organization. *Mol. Biol. Cell.* 18:839–849.

Blumental-Perry, A., C.J. Haney, K.M. Weixel, S.C. Watkins, O.A. Weisz, and M. Aridor. 2006. Phosphatidylinositol 4-phosphate formation at ER exit sites regulates ER export. *Dev. Cell.* 11:671–682.

Bonifacino, J.S., and B.S. Glick. 2004. The mechanisms of vesicle budding and fusion. *Cell.* 116:153–166.

Borgese, N., S. Colombo, and E. Pedrazzini. 2003. The tale of tail-anchored proteins: coming from the cytosol and looking for a membrane. *J. Cell Biol.* 161:1013–1019.

Bretscher, M.S., and S. Munro. 1993. Cholesterol and the Golgi apparatus. *Science.* 261:1280–1281.

Browman, D.T., M.E. Resek, L.D. Zajchowski, and S.M. Robbins. 2006. Erlin-1 and erlin-2 are novel members of the prohibitin family of proteins that define lipid-raft-like domains of the ER. *J. Cell Sci.* 119:3149–3160.

Bulbarelli, A., T. Sprocati, M. Barberi, E. Pedrazzini, and N. Borgese. 2002. Trafficking of tail-anchored Proteins: transport from the endoplasmic reticulum to the plasma membrane and sorting between surface domains in polarised epithelial cells. *J. Cell Sci.* 115:1689–1702.

Campana, V., D. Sarnataro, C. Fasano, P. Casanova, S. Paladino, and C. Zurzolo. 2006. Detergent-resistant membrane domains but not the proteasome are involved in the misfolding of a PrP mutant retained in the endoplasmic reticulum. *J. Cell Sci.* 119:433–442.

Ceppi, P., S. Colombo, M. Francolini, F. Raimondo, N. Borgese, and M. Masserini. 2005. Two tail-anchored protein variants, differing in transmembrane domain length and intracellular sorting, interact differently with lipids. *Proc. Natl. Acad. Sci. USA.* 102:16269–16274.

de Planque, M.R., and J.A. Killian. 2003. Protein-lipid interactions studied with designed transmembrane peptides: role of hydrophobic matching and interfacial anchoring. *Mol. Membr. Biol.* 20:271–284.

Dumas, F., M.C. Lebrun, and J.F. Tocanne. 1999. Is the protein/lipid hydrophobic matching principle relevant to membrane organization and functions? *FEBS Lett.* 458:271–277.

Dunbar, L.A., P. Aronson, and M.J. Caplan. 2000. A transmembrane segment determines the steady-state localization of an ion-transporting adenosine triphosphatase. *J. Cell Biol.* 148:769–778.

Fiedler, K., and J.E. Rothman. 1997. Sorting determinants in the transmembrane domain of p24 proteins. *J. Biol. Chem.* 272:24739–24742.

Fiedler, K., M. Veit, M.A. Stamnes, and J.E. Rothman. 1996. Bimodal interaction of coatomer with the p24 family of putative cargo receptors. *Science.* 273:1396–1399.

Fullekrug, J., J. Boehm, S. Rottger, T. Nilsson, G. Mieskes, and H.D. Schmitt. 1997. Human Rer1 is localized to the Golgi apparatus and complements the deletion of the homologous Rer1 protein of *Saccharomyces cerevisiae*. *Eur. J. Cell Biol.* 74:31–40.

Griffiths, G., A. McDowall, R. Back, and J. Dubochet. 1984. On the preparation of cryosections for immunocytochemistry. *J. Ultrastruct. Res.* 89:65–78.

Hammond, C., and A. Helenius. 1995. Quality control in the secretory pathway. *Curr. Opin. Cell Biol.* 7:523–529.

Hasdemir, B., D.J. Fitzgerald, I.A. Prior, A.V. Tepikin, and R.D. Burgoyne. 2005. Traffic of Kv4 K^+ channels mediated by KChIP1 is via a novel post-ER vesicular pathway. *J. Cell Biol.* 171:459–469.

Honsho, M., J.-y. Mitoma, and A. Ito. 1998. Retention of cytochrome b(5) in the endoplasmic reticulum is transmembrane and luminal domain-dependent. *J. Biol. Chem.* 273:20860–20866.

Iodice, L., S. Sarnataro, and S. Bonatti. 2001. The carboxyl-terminal valine is required for transport of glycoprotein CD8 alpha from the endoplasmic reticulum to the intermediate compartment. *J. Biol. Chem.* 276:28920–28926.

Jackson, M.R., T. Nilsson, and P.A. Peterson. 1993. Retrieval of transmembrane proteins to the endoplasmic reticulum. *J. Cell Biol.* 121:317–333.

Jüschke, C., A. Wächter, B. Schwappach, and M. Seedorf. 2005. *SEC18*/NSF-independent, protein-sorting pathway from the yeast cortical ER to the plasma membrane. *J. Cell Biol.* 169:613–622.

Karhinen, L., R.N. Bastos, E. Jokitalo, and M. Makarow. 2005. Endoplasmic reticulum exit of a secretory glycoprotein in the absence of sec24p family proteins in yeast. *Traffic.* 6:562–574.

Karsten, V., R.S. Hegde, A.P. Sinai, M. Yang, and K.A. Joiner. 2004. Transmembrane domain modulates sorting of membrane proteins in *Toxoplasma gondii*. *J. Biol. Chem.* 279:26052–26057.

Kuismanen, E., and J. Saraste. 1989. Low temperature-induced transport blocks as tools to manipulate membrane traffic. *Methods Cell Biol.* 32:257–274.

Lee, M.C., S. Hamamoto, and R. Schekman. 2002. Ceramide biosynthesis is required for the formation of the oligomeric H+-ATPase Pma1p in the yeast endoplasmic reticulum. *J. Biol. Chem.* 277:22395–22401.

Lee, M.C., E.A. Miller, J. Goldberg, L. Orci, and R. Schekman. 2004. Bidirectional protein transport between the ER and Golgi. *Annu. Rev. Cell Dev. Biol.* 20:87–123.

Letourneur, F., and P. Cosson. 1998. Targeting to the endoplasmic reticulum in yeast cells by determinants present in transmembrane domains. *J. Biol. Chem.* 273:33273–33278.

Lotti, L.V., M.R. Torrisi, M.C. Erra, and S. Bonatti. 1996. Morphological analysis of the transfer of VSV ts-045 G glycoprotein to the intermediate compartment in vero cells. *Exp. Cell Res.* 227:323–331.

Martinez-Menarguez, J.A., H.J. Geuze, J.W. Slot, and J. Klumperman. 1999. Vesicular tubular clusters between the ER and Golgi mediate concentration of soluble secretory proteins by exclusion from COPI-coated vesicles. *Cell.* 98:81–90.

Matsuoka, K., L. Orci, M. Amherdt, S.Y. Bednarek, S. Hamamoto, R. Schekman, and T. Yeung. 1998. COPII-coated vesicle formation reconstituted with purified coat proteins and chemically defined liposomes. *Cell.* 93:263–275.

Mayhew, T., G. Griffiths, A. Habermann, J. Lucocq, N. Emre, and P. Webster. 2003. A simpler way of comparing the labelling densities of cellular compartments illustrated using data from VPARP and LAMP-1 immunogold labelling experiments. *Histochem. Cell Biol.* 119:333–341.

Mezzacasa, A., and A. Helenius. 2002. The transitional ER defines a boundary for quality control in the secretion of ts045 VSV glycoprotein. *Traffic.* 3:833–849.

Mitra, K., I. Ubarretxena-Belandia, T. Taguchi, G. Warren, and D.M. Engelman. 2004. Modulation of the bilayer thickness of exocytic pathway membranes by membrane proteins rather than cholesterol. *Proc. Natl. Acad. Sci. USA.* 101:4083–4088.

Muniz, M., and H. Riezman. 2000. Intracellular transport of GPI-anchored proteins. *EMBO J.* 19:10–15.

Nagai, T., K. Ibata, E.S. Park, M. Kubota, K. Mikoshiba, and A. Miyawaki. 2002. A variant of yellow fluorescent protein with fast and efficient maturation for cell-biological applications. *Nat. Biotechnol.* 20:87–90.

Nehls, S., E.L. Snapp, N.B. Cole, K.J.M. Zaal, A.K. Kenworthy, T.H. Roberts, J. Ellenberg, J.F. Presley, E. Siggia, and J. Lippincott-Schwartz. 2000. Dynamics and retention of misfolded proteins in native ER membranes. *Nat. Cell Biol.* 2:288–295.

Nikonov, A.V., E. Snapp, J. Lippincott-Schwartz, and G. Kreibich. 2002. Active translocon complexes labeled with GFP–Dad1 diffuse slowly as large polysome arrays in the endoplasmic reticulum. *J. Cell Biol.* 158:497–506.

Nishimura, N., and W.E. Balch. 1997. A di-acidic signal required for selective export from the endoplasmic reticulum. *Science.* 277:556–558.

Nufer, O., F. Kappeler, S. Guldbrandsen, and H.P. Hauri. 2003. ER export of ERGIC-53 is controlled by cooperation of targeting determinants in all three of its domains. *J. Cell Sci.* 116:4429–4440.

Pathre, P., K. Shome, A. Blumental-Perry, A. Bielli, C.J. Haney, S. Alber, S.C. Watkins, G. Romero, and M. Aridor. 2003. Activation of phospholipase D by the small GTPase Sar1p is required to support COPII assembly and ER export. *EMBO J.* 22:4059–4069.

Pedrazzini, E., A. Villa, and N. Borgese. 1996. A mutant cytochrome b_5 with a lengthened membrane anchor escapes from the endoplasmic reticulum and reaches the plasma membrane. *Proc. Natl. Acad. Sci. USA.* 93:4207–4212.

Pedrazzini, E., A. Villa, R. Longhi, A. Bulbarelli, and N. Borgese. 2000. Mechanism of residence of cytochrome b(5), a tail-anchored protein, in the endoplasmic reticulum. *J. Cell Biol.* 148:899–914.

Pentcheva, T., E.T. Spiliotis, and M. Edidin. 2002. Cutting edge: Tapasin is retained in the endoplasmic reticulum by dynamic clustering and exclusion from endoplasmic reticulum exit sites. *J. Immunol.* 168:1538–1541.

Presley, J.F., N.B. Cole, T.A. Schroer, K. Hirschberg, K.J. Zaal, and J. Lippincott-Schwartz. 1997. ER-to-Golgi transport visualized in living cells. *Nature.* 389:440–441.

Rizzo, M.A., G.H. Springer, B. Granada, and D.W. Piston. 2004. An improved cyan fluorescent protein variant useful for FRET. *Nat. Biotechnol.* 22:445–449.

Rosenwald, A.G., C.E. Machamer, and R.E. Pagano. 1992. Effects of a sphingolipid synthesis inhibitor on membrane transport through the secretory pathway. *Biochemistry.* 31:3581–3590.

Runz, H., K. Miura, M. Weiss, and R. Pepperkok. 2006. Sterols regulate ER-export dynamics of secretory cargo protein ts-O45-G. *EMBO J.* 25:2953–2965.

Saraste, J., G.E. Palade, and M.G. Farquhar. 1987. Antibodies to rat pancreas Golgi subfractions: identification of a 58-kD cis-Golgi protein. *J. Cell Biol.* 105:2021–2029.

Sato, K., M. Sato, and A. Nakano. 1997. Rer1p as common machinery for the endoplasmic reticulum localization of membrane proteins. *Proc. Natl. Acad. Sci. USA.* 94:9693–9698.

Sato, K., M. Sato, and A. Nakano. 2003. Rer1p, a retrieval receptor for ER membrane proteins, recognizes transmembrane domains in multiple modes. *Mol. Biol. Cell.* 14:3605–3616.

Scales, S.J., R. Pepperkok, and T.E. Kreis. 1997. Visualization of ER-to-Golgi transport in living cells reveals a sequential mode of action for COPII and COPI. *Cell.* 90:1137–1148.

Schamel, W.W.A., S. Kuppig, B. Becker, K. Gimborn, H.P. Hauri, and M. Reth. 2003. A high-molecular-weight complex of membrane proteins BAP29/31 is involved in the retention of membrane-bound IgD in the endoplasmic reticulum. *Proc. Natl. Acad. Sci. USA.* 100:9861–9866.

Schweizer, A., J.A.M. Fransen, T. Bachi, L. Ginsel, and H.-P. Hauri. 1988. Identification, by a monoclonal antibody, of a 53-kD protein associated with a tubulo-vesicular compartment at the cis-side of the Golgi apparatus. *J. Cell Biol.* 107:1643–1653.

Siggia, E.D., J. Lippincott-Schwartz, and S. Bekiranov. 2000. Diffusion in inhomogeneous media: theory and simulations applied to whole cell photobleach recovery. *Biophys. J.* 79:1761–1770.

Smith, D.C., D.J. Sillence, T. Falguieres, R.M. Jarvis, L. Johannes, J.M. Lord, F.M. Platt, and L.M. Roberts. 2006. The association of Shiga-like toxin with detergent-resistant membranes is modulated by glucosylceramide and is an essential requirement in the endoplasmic reticulum for a cytotoxic effect. *Mol. Biol. Cell.* 17:1375–1387.

Snapp, E.L., N. Altan, and J. Lippincott-Schwartz. 2003a. Measuring protein mobility by photobleaching GFP chimeras in living cells. *Curr. Protoc. Cell Biol.* Chapter 21:Unit 21.1.

Snapp, E.L., R.S. Hegde, M. Francolini, F. Lombardo, S. Colombo, E. Pedrazzini, N. Borgese, and J. Lippincott-Schwartz. 2003b. Formation of stacked ER cisternae by low affinity protein interactions. *J. Cell Biol.* 163:257–269.

Sprong, H., P. van der Sluijs, and G. van Meer. 2001. How proteins move lipids and lipids move proteins. *Nat. Rev. Mol. Cell Biol.* 2:504–513.

Stornaiuolo, M., L.V. Lotti, N. Borgese, M.-R. Torrisi, G. Mottola, G. Martire, and S. Bonatti. 2003. The KDEL and KKXX retrieval signals appended to the same reporter protein determine different trafficking between endoplasmic reticulum, intermediate compartment and Golgi complex. *Mol. Biol. Cell.* 14:889–902.

Sturbois-Balcerzak, B., P. Vincent, L. Maneta-Peyret, M. Duvert, B. Satiat-Jeunemaitre, C. Cassagne, and P. Moreau. 1999. ATP-dependent formation of phosphatidylserine-rich vesicles from the endoplasmic reticulum of leek cells. *Plant Physiol.* 120:245–256.

Tartakoff, A.M. 1986. Temperature and energy dependence of secretory protein transport in the exocrine pancreas. *EMBO J.* 5:1477–1482.

Voeltz, G.K., W.A. Prinz, Y. Shibata, J.M. Rist, and T.A. Rapoport. 2006. A class of membrane proteins shaping the tubular endoplasmic reticulum. *Cell.* 124:573–586.

Wang, J.M., L. Zhang, Y. Yao, N. Viroonchatapan, E. Rothe, and Z.Z. Wang. 2002. A transmembrane motif governs the surface trafficking of nicotinic acetylcholine receptors. *Nat. Neurosci.* 5:963–970.

Watson, P., and D.J. Stephens. 2005. ER-to-Golgi transport: form and formation of vesicular and tubular carriers. *Biochim. Biophys. Acta.* 1744:304–315.

Watson, P., A.K. Townley, P. Koka, K.J. Palmer, and D.J. Stephens. 2006. Sec16 defines endoplasmic reticulum exit sites and is required for secretory cargo export in mammalian cells. *Traffic.* 7:1678–1687.